

A finite state model for respiratory motion analysis in image guided radiation therapy

Huanmei Wu¹, Gregory C Sharp², Betty Salzberg¹, David Kaeli³, Hiroki Shirato⁴ and Steve B Jiang²

¹ College of Computer and Information Science, Northeastern University, Boston, MA 02115, USA

² Department of Radiation Oncology, Massachusetts General Hospital and Harvard Medical School, Boston, MA 02114, USA

³ Department of Electrical and Computer Engineering, Northeastern University, Boston, MA 02115, USA

⁴ Department of Radiation Medicine, Hokkaido University School of Medicine, Sapporo, Japan

E-mail: maggiewu@ccs.neu.edu

Received 16 August 2004, in final form 18 October 2004

Published 19 November 2004

Online at stacks.iop.org/PMB/49/5357

doi:10.1088/0031-9155/49/23/012

Abstract

Effective image guided radiation treatment of a moving tumour requires adequate information on respiratory motion characteristics. For margin expansion, beam tracking and respiratory gating, the tumour motion must be quantified for pretreatment planning and monitored on-line. We propose a finite state model for respiratory motion analysis that captures our natural understanding of breathing stages. In this model, a regular breathing cycle is represented by three line segments, exhale, end-of-exhale and inhale, while abnormal breathing is represented by an irregular breathing state. In addition, we describe an on-line implementation of this model in one dimension. We found this model can accurately characterize a wide variety of patient breathing patterns. This model was used to describe the respiratory motion for 23 patients with peak-to-peak motion greater than 7 mm. The average root mean square error over all patients was less than 1 mm and no patient has an error worse than 1.5 mm. Our model provides a convenient tool to quantify respiratory motion characteristics, such as patterns of frequency changes and amplitude changes, and can be applied to internal or external motion, including internal tumour position, abdominal surface, diaphragm, spirometry and other surrogates.

1. Introduction

While modern radiation therapy treatments are capable of delivering highly conformal doses, the conformality of dose that can be delivered to thoracic and abdominal lesions is degraded

by respiratory motion (Bortfeld *et al* 2002, Jiang *et al* 2003, Bortfeld and Jiang 2004, Goitein 2004). A variety of treatment techniques have been developed or are under development for motion compensation, including margin expansion, breath holding, respiratory gating and beam tracking (Mageras and Yorke 2004, Murphy 2004, van Herk 2004). All these motion compensation methods, except for breath holding, require an adequate understanding of the motion characteristics. In particular, if treatment is to be delivered using a beam tracking technique, the important parameters of the tumour trajectory must be quantified during simulation so they may be used in treatment planning (Neicu *et al* 2003). Furthermore, these quantities must be continually monitored during treatment to ensure proper treatment delivery.

The best parametrization for describing respiratory motion remains an open question. However, it seems clear that at least the amplitude and stability of the motion must be quantified for designing margins (van Herk 2004), and the reproducibility of position in the gating window must be quantified for designing a gated treatment (Mageras and Yorke 2004). The breathing period and waveform characteristics are useful for planning treatments that use beam tracking (Keall *et al* 2001, Neicu *et al* 2003, Murphy 2004, Suh *et al* 2004). Already there exist several methods that address different aspects of this problem. Lujan *et al* and Seppenwoolde *et al* describe a method of modelling a breathing pattern with a modified cosine function (Lujan *et al* 1999, Seppenwoolde *et al* 2002). This approach gives excellent fits for breathing patterns when inhale and exhale phases are symmetrical. Neicu *et al* have described how to capture a more detailed waveform model using a concept called the average tumour trajectory (Neicu *et al* 2003). In their work, the minima and maxima in the superior–inferior direction are matched, and the waveform is normalized and averaged to better describe the characteristic motion.

The goal of this work is to design a quantitative method for describing breathing motion that captures all of the natural characteristics, and can be used for both off-line analysis and on-line monitoring. To achieve this goal, we have designed and implemented a finite state model that characterizes a breathing cycle, as containing three breathing states: exhale (EX), end-of-exhale (EOE) and inhale (IN). These three states are expected to repeat in succession as they do in natural breathing. Any motion that does not belong to any of the above three states will be treated as irregular breathing, a fourth state (IRR).

We have implemented this model in one dimension, and evaluated its fidelity on the lung tumour motion of 23 patients with peak-to-peak tumour motion greater than 7 mm (Shirato *et al* 2000). We found the model can accurately characterize a wide variety of patient breathing patterns with an average RMS error less than 1 mm. The finite state model also provides a convenient tool for statistical analysis of motion characteristics, such as amplitude changes, frequency changes and motion stability.

2. Methods

This section discusses our method for respiratory motion analysis in image guided radiation therapy. First, we introduce the finite state model for motion analysis, and then describe an on-line implementation.

2.1. Motion modelling

The finite state model for respiratory motion analysis is based on our natural understanding of breathing motion and the requirements of motion compensated treatment. As a patient inhales and exhales, a target moves in a periodic pattern as illustrated in figure 1(a). For regular

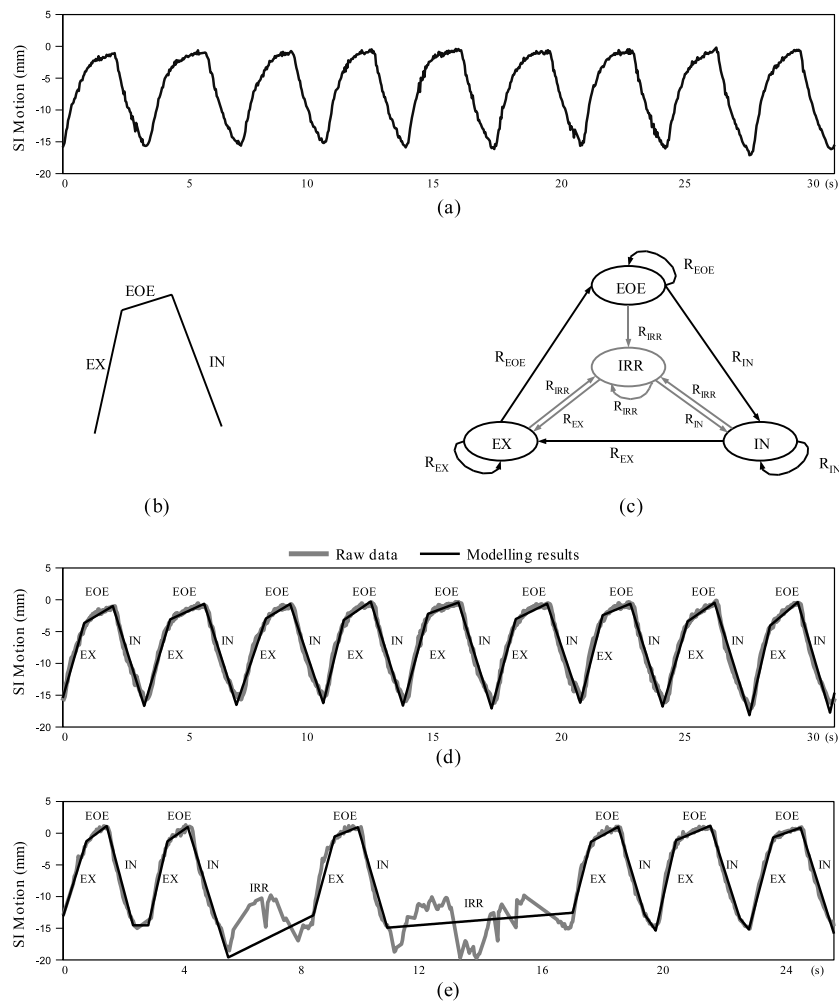


Figure 1. The finite state model for tumour respiratory motion: (a) raw data of tumour motion, (b) three states of a regular breathing cycle, (c) finite state automaton for respiratory motion, (d) regular breathing with three states per breathing cycle and (e) respiratory motion with irregular breathing.

breathing, the target motion corresponds to lung deflation, rest after lung deflation and lung expansion. Irregular breathing can occur at any time during any of the above actions. These motion patterns are modelled using three regular breathing states: exhale (EX), end-of-exhale (EOE) and inhale (IN), and one irregular breathing state (IRR). A single regular breathing cycle has exactly three breathing states, i.e., EX, EOE and IN, as shown in figure 1(b). Motion proceeds from state to state in a fixed order:

$$\dots \Rightarrow \text{EX} \Rightarrow \text{EOE} \Rightarrow \text{IN} \Rightarrow \text{EX} \Rightarrow \dots$$

Each of these states corresponds to a natural action: EX is the motion due to lung deflation, EOE is the motion for rest after lung deflation and IN is the motion due to lung expansion. An example of segmentation into these three states is illustrated in figure 1(d).

When a patient breathes abnormally, the respiratory motion does not fall into any of the three regular breathing states. The irregular state (IRR) is introduced to solve this problem.

The IRR is entered during irregular breathing, and is left when regular breathing resumes. An example of respiratory motion with irregular breathing is demonstrated in figure 1(e), which also shows the corresponding finite state representation by the four breathing states.

The transition from one state to another is guided by the *finite state automaton* (FSA) illustrated in figure 1(c). An FSA is an abstract machine that has a finite set of states and transitions between states. When new data arrive, the machine determines whether the tumour has transited to a next state or not. The finite state machine can begin or end in any state.

State transitions are primarily triggered by the motion velocity changes. Each state has an expected range of velocities, although the ranges for the different states overlap. Upon receipt of a new data point, a set of rules is used to decide if the tumour will stay at the current state or transit to another state. The details of the state transition rules will be described in section 2.3.

2.2. Preliminaries

This section will summarize some common notation and the fitting methods used in this paper. For generality, the corresponding notation are defined in N -dimensional space, so they can be used for 1D, 2D and 3D breathing motions. The upper-case bold italic characters, such as \mathbf{V} or \mathbf{X} , represent vectors and directed line segments, while lower-case italic letters, such as x_0 or $v(t_0 \rightarrow t_1)$, represent scalars.

Points. An n -dimensional point at time t is represented by a vector from the origin,

$$\mathbf{X}(t) = \{x_0, x_1, \dots, x_n\}.$$

Directed line segments. A directed line segment in n -D from point $\mathbf{X}(t_0)$ to $\mathbf{X}(t_1)$ is defined as

$$\mathbf{L} = \overrightarrow{X_0 X_1} = \mathbf{X}(t_1) - \mathbf{X}(t_0) = \{\mathbf{X} \mid \mathbf{X} = \mathbf{X}_0 + \mathbf{V} \cdot t\},$$

where $t_0 \leq t \leq t_1$ and \mathbf{V} is the velocity of $\overrightarrow{X_0 X_1}$ (see below).

Line segment length. The length of a directed line segment from $\mathbf{X}(t_0)$ to $\mathbf{X}(t_1)$ is denoted as $\|\overrightarrow{X_0 X_1}\|$ and is defined as

$$\|\overrightarrow{X_0 X_1}\| = \sqrt{\sum_{i=1}^n (x_{1i} - x_{0i})^2}.$$

Velocity. The velocity from point $\mathbf{X}(t_0)$ to point $\mathbf{X}(t_1)$ is calculated from the following formula:

$$\mathbf{V}(t_0 \rightarrow t_1) = \frac{\overrightarrow{X_0 X_1}}{t_1 - t_0} = \frac{\mathbf{X}(t_1) - \mathbf{X}(t_0)}{t_1 - t_0}.$$

Speed. The speed of tumour motion is the magnitude of the corresponding velocity,

$$v(t_0 \rightarrow t_1) = \frac{\|\overrightarrow{X_0 X_1}\|}{t_1 - t_0}.$$

Amplitude. The average amplitude for two connected directed line segments \mathbf{L}_1 and \mathbf{L}_2 , where the initial point of \mathbf{L}_2 is the final point of \mathbf{L}_1 , is defined as

$$\Lambda(\mathbf{L}_1, \mathbf{L}_2) = \frac{\|\mathbf{L}_1\| + \|\mathbf{L}_2\|}{2}.$$

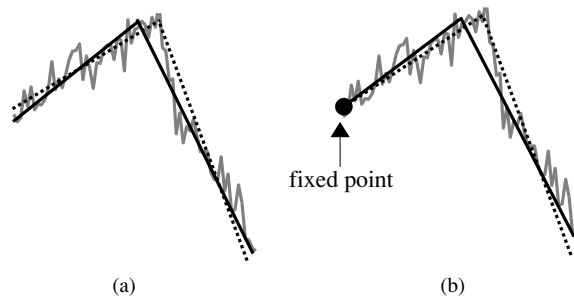


Figure 2. Linear spline fit: (a) free spline fit and (b) partial spline fit.

Angle of velocity change. The angle between two velocities is $\Theta(\mathbf{V}_1, \mathbf{V}_2)$ and calculated by

$$\Theta(\mathbf{V}_1, \mathbf{V}_2) = \arccos\left(\frac{\mathbf{V}_1 \cdot \mathbf{V}_2}{\|\mathbf{V}_1\| \|\mathbf{V}_2\|}\right),$$

where $\mathbf{V}_1 \cdot \mathbf{V}_2$ is the dot product of the two vectors.

Least square fit. Given a set of data points $\{\mathbf{Y}(t_1), \mathbf{Y}(t_2), \dots, \mathbf{Y}(t_m)\}$, we may seek a directed line segment $\overrightarrow{X_1 X_m}$ that best fits the given points. We use least-squares fit which minimizes the square of differences σ^2 between the corresponding points of $\overrightarrow{X_1 X_m}$ and the given points, where

$$\sigma^2 = \sum_{i=1}^m (\mathbf{X}(t_i) - \mathbf{Y}(t_i))^2.$$

Linear spline fit. A spline fit is a data analysis technique for estimating (via the least-squares criterion) the parameters in a spline polynomial model. In our method, a linear spline fit comprising two connected line segments is used for optimization. Two different situations of spline fitting are used: a free spline fit and a partial spline fit. As shown in figure 2, the free spline fit has no constraints on either of the two line segments, while the partial spline fit constrains the first knot of the first line segment to a certain prefixed point. The applications of these two spline fitting methods will be discussed in section 2.3.

Sliding window algorithm. A sliding window refers to selecting a subset of data. We use a variable-length sliding window that includes the data points from the three most recent line segments. Whenever a new knot is created, the window will move forward by one knot. New line segments can only be generated within the current sliding window. Previous line segments will not be changed by subsequent processing.

Decisive line segments. There are two line segments which are important in the state transitions. One is the most recent line segment \mathbf{L}_f , as shown in figure 3(a). \mathbf{L}_f is a least-squares fit of all the data points after last state transition point, and represents the tumour's current moving state. The other is the decision line segment. When a new data point arrives, a short directed line segment is fit to the K most recent points. This line segment is called the decision line segment and is denoted by \mathbf{L}_d . These two line segments and their velocities are used to determine whether or not a new state has occurred.

Variables and symbols. To describe our algorithm, we introduce the following variables and symbols. Θ_c and Λ_c are two adjustable thresholds used for testing velocity change and

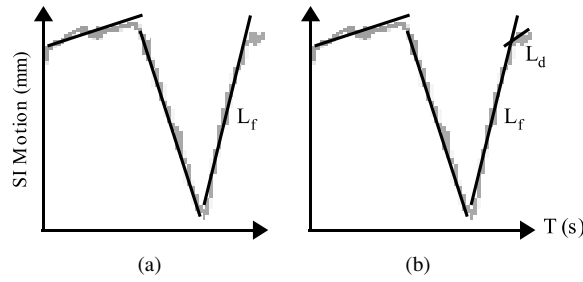


Figure 3. The most recent line segment L_f and the decision line segment L_d .

Table 1. Symbols and variables.

Symbols	Descriptions	Symbols	Descriptions
Θ_c	Velocity threshold	Λ_c	Amplitude threshold
L_f	The most recent line segment	L_d	The decisive line segment
V_f	The velocity of L_f	V_d	The velocity of L_d
S_f	The breathing state of L_f	L_{f-i}	The i th line segment before L_f
R_S	The velocity range of state S	next(S)	The next regular state after S

amplitude. L_f and L_d are the decisive line segments described above. V_f and V_d are the corresponding velocities of L_f and L_d . S_f is the breathing state of L_f . The i th line segment before L_f is denoted as L_{f-i} . R_S is the velocity range of state S (i.e., R_{EX} , R_{EOE} , R_{IN} or R_{IRR}). When S is a regular breathing state, the next regular breathing state after state S is denoted as next(S). These symbols are summarized in table 1.

2.3. Algorithm

The overall flow and decision making of our on-line algorithm is illustrated in figure 4. When each data point arrives, a decision line is generated from the data in the sliding window. Various properties of the decision line are tested against a set of rules to identify if a state transition has occurred, as summarized in table 2. Nine different actions, marked A through I, are possible. These actions control state transitions, including a possible retrospective modification of the three most recent line segments. We will now give a more detailed explanation for each action in figure 4 and table 2.

(A) *Decision line generation.* When a new data point arrives, a new decision line segment L_d is generated, and its velocity V_d is computed. By comparing L_d and V_d with the last line segment, L_f and V_f , different decisions for state transitions will be taken.

The decision rules follow the flow in figure 4. For a tumour in the irregular state ($S_f = IRR$), we only test whether the tumour has resumed regular breathing or not. If it has, we update the current state; otherwise, we continue in the IRR state. For a tumour in one of the regular breathing states, we test if the velocity difference, $\Theta(V_f, V_d)$, is less than Θ_c . If so, there will be no state transition. Otherwise, V_d is compared with the range of velocities allowed by the next regular state of the finite state model. If it is in range, the amplitudes of the last two line segments are checked to see if the previous greedy transition should be retracted. Only if the decision line L_d has passed these tests for state and amplitude will a new line segment be generated.

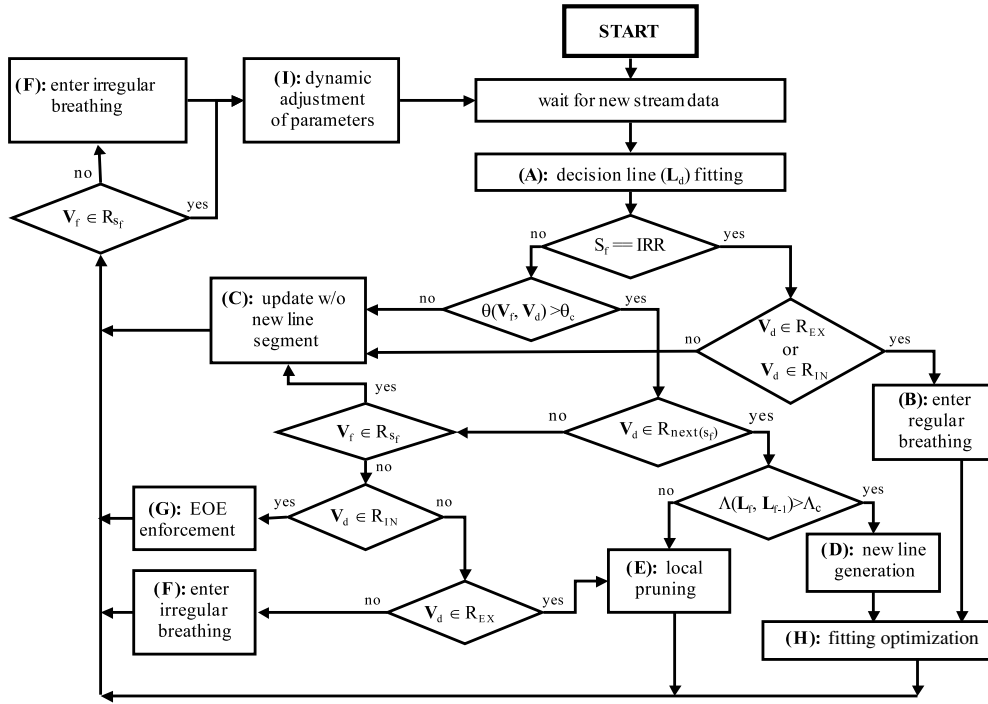


Figure 4. Algorithmic flow of on-line segmentation process.

Table 2. Decision rules.

Rule	Conditions	Decisions
1	$S_f = \text{IRR}$ and $(V_d \in R_{\text{EX}}$ or $V_d \in R_{\text{IN}})$	B: Enter regular breathing
2	$S_f \neq \text{IRR}$ and $\Theta(V_f, V_d) \leq \Theta_c$	
3	$S_f = \text{IRR}$ and $V_d \notin R_{\text{EX}}$ and $V_d \notin R_{\text{IN}}$	C: Update without new line segment
4	$S_f \neq \text{IRR}$ and $\Theta(V_f, V_d) > \Theta_c$ and $V_d \notin R_{\text{next}(S_f)}$ and $V_d \in R_{S_f}$	
5	$S_f \neq \text{IRR}$ and $\Theta(V_f, V_d) > \Theta_c$ and $V_d \in R_{\text{next}(S_f)}$ and $\Lambda(L_f, L_{f-1}) > \Lambda_c$	D: New line generation
6	$S_f \neq \text{IRR}$ and $\Theta(V_f, V_d) > \Theta_c$ and $V_d \notin R_{\text{next}(S_f)}$ and $V_d \notin R_{S_f}$ and $V_d \in R_{\text{EX}}$	
7	$S_f \neq \text{IRR}$ and $\Theta(V_f, V_d) > \Theta_c$ and $V_d \in R_{\text{next}(S_f)}$ and $\Lambda(L_f, L_{f-1}) \leq \Lambda_c$	E: Local pruning
8	$S_f \neq \text{IRR}$ and $\Theta(V_f, V_d) > \Theta_c$ and $V_d \notin R_{\text{next}(S_f)}$ and $V_d \notin R_{S_f}$ and $V_d \notin R_{\text{EX}}$ and $V_d \notin R_{\text{IN}}$	F: Enter irregular breathing
9	$S_f \notin R_{S_f}$	
10	$S_f \neq \text{IRR}$ and $\Theta(V_f, V_d) > \Theta_c$ and $V_d \notin R_{\text{next}(S_f)}$ and $V_d \notin R_{S_f}$ and $V_d \in R_{\text{IN}}$	G: EOE enforcement

(B) *Resumption of regular breathing.* This action defines the transition from IRR state to normal breathing. Because of large variations of velocity changes in the EOE state, we only transition from IRR to regular breathing in the EX or IN state. Resumption of regular

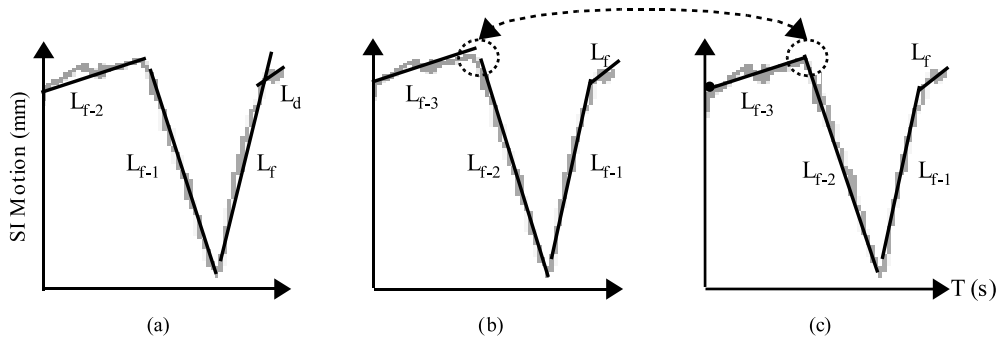


Figure 5. New line generation and fitting optimization: (a) rule checking, (b) new line generation and (c) local optimization.

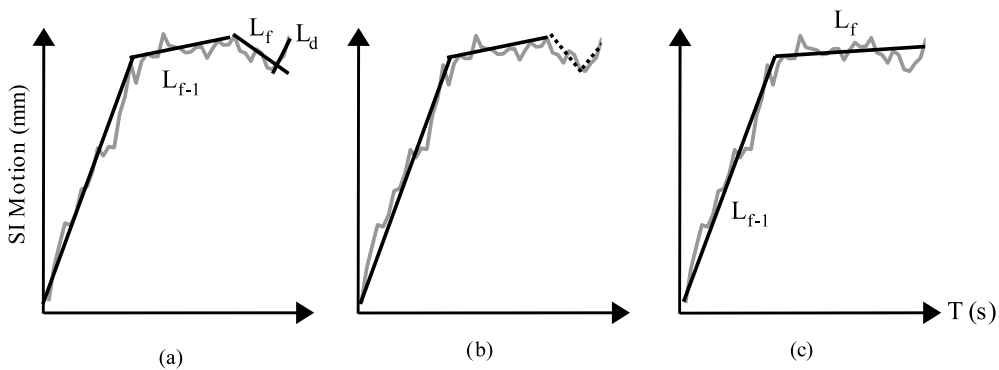


Figure 6. Amplitude checking and local pruning: (a) rule checking, (b) without amplitude checking and (c) with amplitude checking and local pruning.

breathing follows the same rules as initial state identification. A free spline fit is used to generate a new line segment, which becomes the first regular breathing state.

- (C) *Update without new line segment.* If there is no need to generate a new line segment or to modify other existing line segments, new data point is added to the most recent existing line segment L_f . There are three situations that require only this simple update. The first case is that the tumour is in irregular breathing and it has not resumed regular breathing. The second case is that the tumour is in a regular breathing state and the velocity has no significant changes. The third case occurs when there is significant velocity change, but the decision velocity V_d does not fall within the velocity range of the next regular state of S_f and still lies within the velocity range of the current state.
- (D) *New line generation.* When a motion transition from one state to another has occurred, a new line segment will be generated to represent the new motion state. This process is illustrated in figure 5. First, a free spline fit is applied to the points covered by the previous line segment L_f and the decision line segment L_d . As shown in figure 5(b), the new line segment becomes the new L_f , and the previous line segment becomes L_{f-1} . Finally, a local optimization over line segments L_{f-2} and L_{f-3} is performed, as will be discussed in action (H).
- (E) *Local pruning.* Local pruning is an action that combines the last two line segments, L_f and L_{f-1} , when velocity change is more than Θ_c , but the amplitude change of the previous two line segments is less than Λ_c . This process is illustrated in figure 6. The

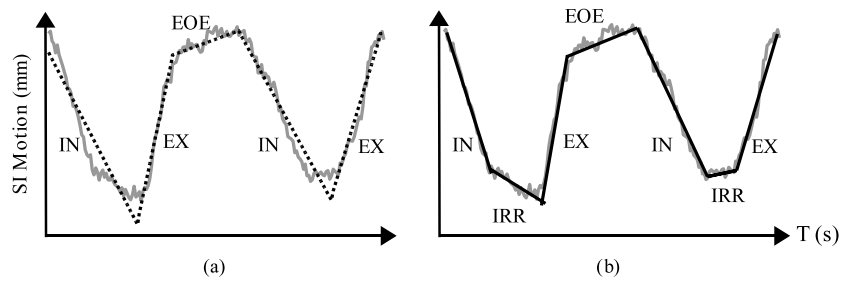


Figure 7. Irregular breathing handling: (a) without IRR state and (b) with IRR state.

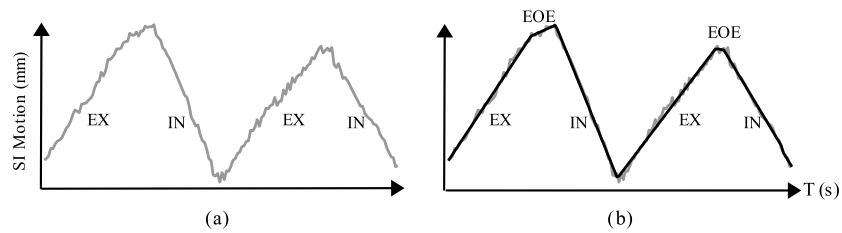


Figure 8. Enforcement of EOE state: (a) alternate exhale and inhale and (b) with EOE enforcement.

dotted line shows that without amplitude checking, an undesired new line segment can be generated. Local pruning allows backtracking when this situation occurs. The segments L_{f-1} , L_f and L_d are replaced with a single-line segment, which becomes the new L_f . The state of the new L_f is the same as that of the original L_{f-1} .

- (F) *Entering irregular breathing.* There are two cases when a tumour enters irregular breathing. One case is that tumour has extended breathing hold after the IN state. An example is shown in figure 7. The dotted line segments in figure 7(a) show the line segments that would be generated if we use only the three regular breathing states. The fitting quality is much worse than the fitting quality with an irregular breathing state (figure 7(b)).

The other irregular breathing case occurs when the velocity of the final line segment does not match the allowed velocities of its corresponding state. In this case, the last line segment will be marked as IRR state.

- (G) *EOE enforcement.* Another characteristic breathing pattern exists where the patient breathing seems to alternate between inhale and exhale states, and lacks a true EOE state. An example is shown in figure 8. The EOE enforcement action is used to ensure that an EOE line segment is generated at the transition from EX to IN. The minimum length of an EOE state is a tunable parameter, which we have set to 133 ms (4 data points for 30 Hz imaging rate).
- (H) *Fitting optimization.* Using a free spline fit for new line segment generation, it is possible that two adjacent line segments are not well connected at the given separating point. This situation is clearly observed in figure 5(b). Modification of the line fitting parameters of L_{f-2} and L_{f-3} is required to make sure that the line segments are well connected. The optimization process is performed using a partial spline fit, with the beginning point of L_{f-3} fixed during fitting. The result of this optimization process is demonstrated in figure 5(c). After local optimization, line segment L_{f-3} is frozen, and will not be modified again by any later process. Note that because the transition point may change, L_{f-2} changes during the optimization of L_{f-1} .

- (I) *Dynamic adaptation.* Because of motion complexity, tumours can have amplitude changes, baseline shifting and period changes. The thresholds Θ_c and Λ_c for testing velocity change and amplitude will change dynamically during on-line data processing. At the beginning, these thresholds are initialized to default values. As more and more data arrive, the thresholds change to adapt to the most recent breathing patterns. In our one-dimensional implementation, the threshold on amplitude, Λ_c , is initialized to 4 mm for superior–inferior motion more than 7 mm. As data are processed, Λ_c tracks one-third of the magnitude of the EX or IN states, averaged over the last four breathing periods. Similarly, Θ_c is initialized to 4.5 mm s^{-1} , and dynamically changes to match one quarter of the average velocity of the EX state.

3. Materials

We performed this study retrospectively using lung tumour movement data of patients treated using the real-time tumour-tracking radiation therapy (TRRT) system at Hokkaido University (Seppenwoolde *et al* 2002, Shirato *et al* 2000a, 2000b). In this system, a 2 mm or 1.5 mm diameter gold marker is inserted into or near the lung tumour using image guided implantation. The system can detect the actual marker position at a rate of 30 Hz using two x-ray imaging systems. It uses fluoroscopy image processor units to determine the 3D position of the implanted marker and employs automatic pattern recognition of the markers in real time. The geometric accuracy of the tumour-tracking system is better than 1.5 mm. Lung tumour motion data of 42 patients treated between 2001 and 2002 were analysed. From these, 23 patients with breathing amplitude greater than 7 mm were identified and used to evaluate fitting quality and to analyse motion patterns.

A qualitative examination of the tumour motion patterns and signal quality of 23 patients shows that there are significant differences between patients. An example of the breathing signals from six different patients is shown in figure 9. Figure 9(a) shows a breathing pattern that is regular in both period and amplitude. Figure 9(b) shows the motion of a tumour where the breathing frequency changes over time. Figure 9(c) illustrates a breathing pattern with base line shifts. Figure 9(d) displays a tumour motion with amplitude changes. Figure 9(e) highlights the fact that the raw tracking signal is often noisy due to cardiac motion. Figure 9(f) demonstrates a breathing pattern where both the exhale home position and the amplitude drift over time. These motion patterns are well characterized by our finite state model.

A more detailed observation shows that there are other breathing cycle patterns, as illustrated in figure 10. A breathing cycle with three breathing states, as shown in figure 10(a), is the most general case, comprising approximate 85% of our breathing data. About 10% of the patients only have exhale and inhale states, or with a very short end-of-exhale state, which is illustrated in figure 10(b). About 5% patients breathe with an additional relaxation state after inhale as shown in figure 10(c). Figure 10(d) displays a special breathing pattern, where there are two end-of-exhale states, separated by a short inhale-like state. Some patients have more complicated breathing signals which incorporate several breathing state patterns. As illustrated in figure 10(e), a patient can alternate between 2-state, 3-state and 4-state motions.

4. Results and discussion

In this section, we will discuss the advantages of this finite state model, the quality of our on-line implementation, an application of the analysis results and some drawbacks of our model.

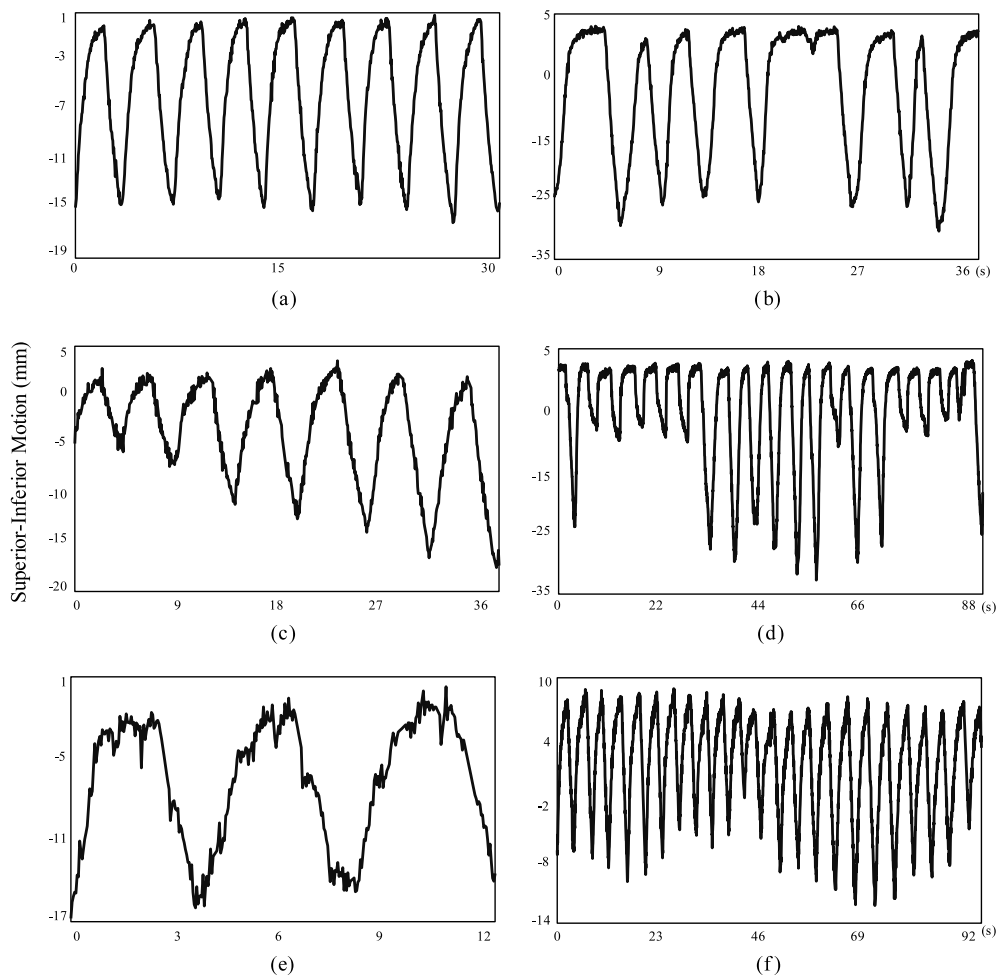


Figure 9. Tumour motion and data quality: (a) regular breathing, (b) frequency changes, (c) baseline shifts, (d) amplitude changes, (e) cardiac motion and (f) combinations.

The idea of using three states to model a regular breathing cycle has several advantages. First, it fits well with our natural understanding of tumour respiratory motion. Second, it provides a convenient way to characterize the motion of the EOE state, usually used as gating window in gated treatment. The model also provides a convenient way to summarize and compare statistical information for different states, which can be used in dynamic treatment planning during real-time radiotherapy or radiosurgery. Third, the piecewise linear representation of raw streams saves storage and will produce fast retrieval of historical medical information. Fourth, our implementation algorithm of the finite state model works in an on-line fashion. The algorithm only requires constant space and runs in linear time. The line segment of current respiration can be determined in real time. The average processing time for each new measurement is less than 1 ms. The quick response time is a big advantage for its application in real-time radiotherapy. Finally, this model is suitable for both on-line subsequence similarity matching and offline patient similarity analysis.

The root mean square (RMS) errors of the on-line fitting for 23 different patients and their average RMS errors are shown in figure 11. The average RMS error is less than 1 mm

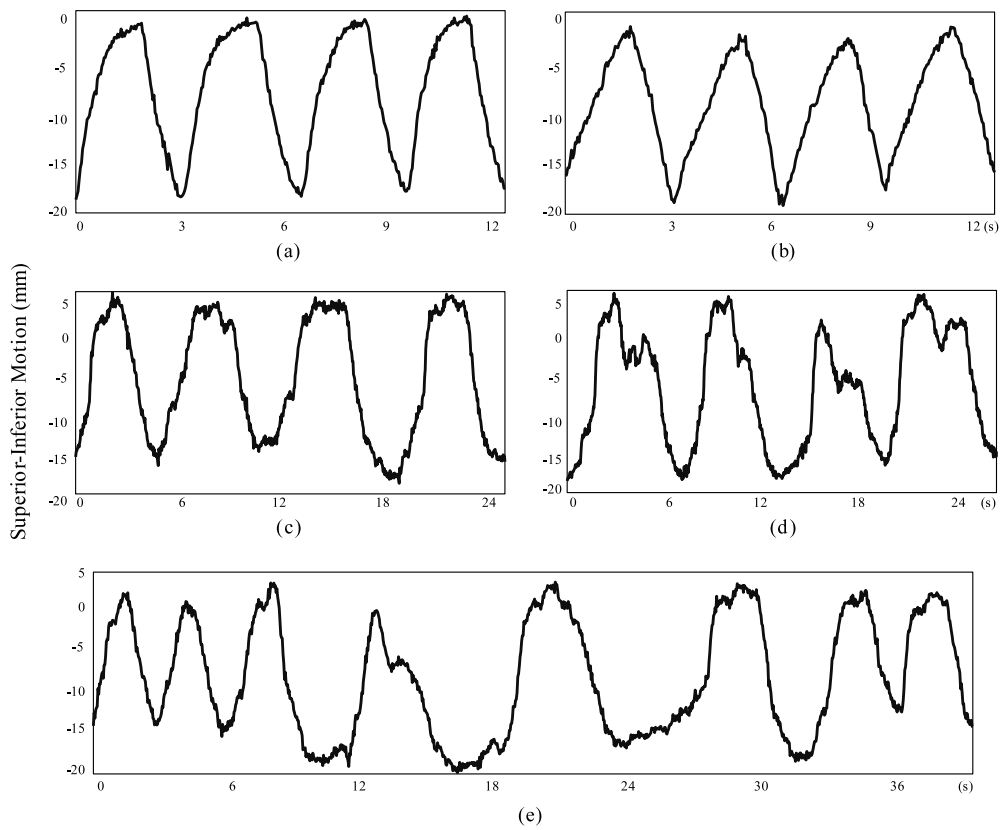


Figure 10. Common and unusual breathing patterns: (a) three breathing states, (b) two breathing states, (c) four breathing states, (d) special breathing states and (e) combinations of all breathing states.

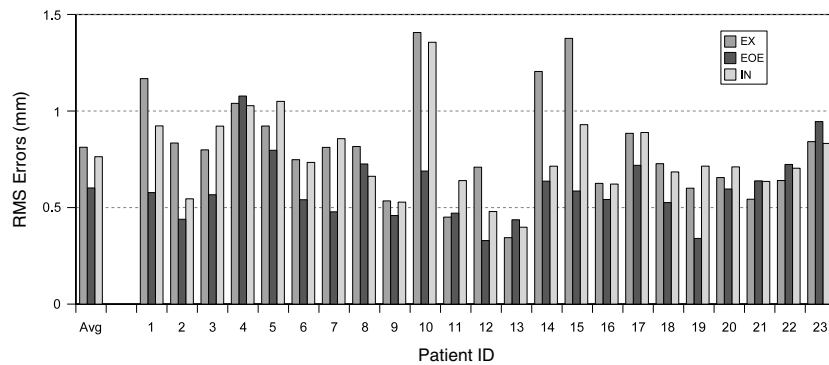


Figure 11. Fidelity of our model to raw data.

on average and less than 1.5 mm for all patients. As demonstrated in figure 11, most patients have the smallest RMS error in the EOE state. The RMS errors for exhale and inhale states are quite similar, with a little variation for different patients. This pattern of the RMS errors can be explained by the motion pattern of tumours. Tumours have less movement in the EOE state, while larger movements in exhale and inhale states.

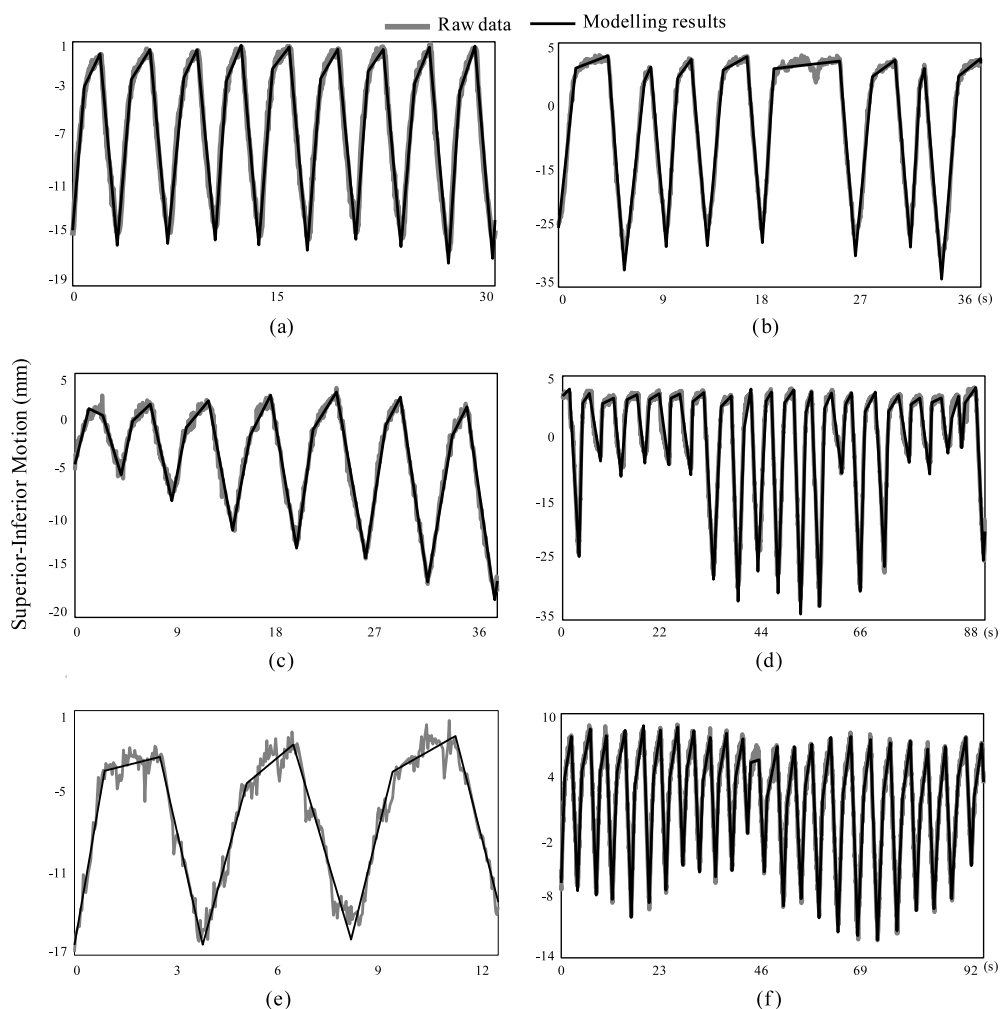


Figure 12. Modelling results of different breathing patterns and data qualities: (a) regular breathing, (b) frequency changes, (c) baseline shifts, (d) amplitude changes, (e) cardiac motion and (f) combinations.

The finite state model works not only for tumour motion with regular breathing patterns, it produces good fitting results even for patients who have very complex breathing patterns, such as breathing with frequency changes, amplitude changes, base line shifting, or the combination of all the variations. It also works well for patients with different breathing cycle patterns, such as two-state, three-state, four-state, or the combinations of all the different patterns. Figures 12 and 13 display the modelling results of the respiratory motion in figures 9 and 10. The final line segments seem to be a qualitatively good representation of the raw data.

The three-state motion model gives convenient ways to summarize and analyse motion characteristics. Figure 14 presents the different breathing lengths for each state. The average time across patients shows that the EOE state is the longest breathing phase, and exhale and inhale states have shorter length. For some patients, such as patients 11 and 13, EOE is the shortest phase of breathing. Other patients have equal breathing time for each of the three states, such as patients 4 and 19. Yet other patients have the breathing time in the order of

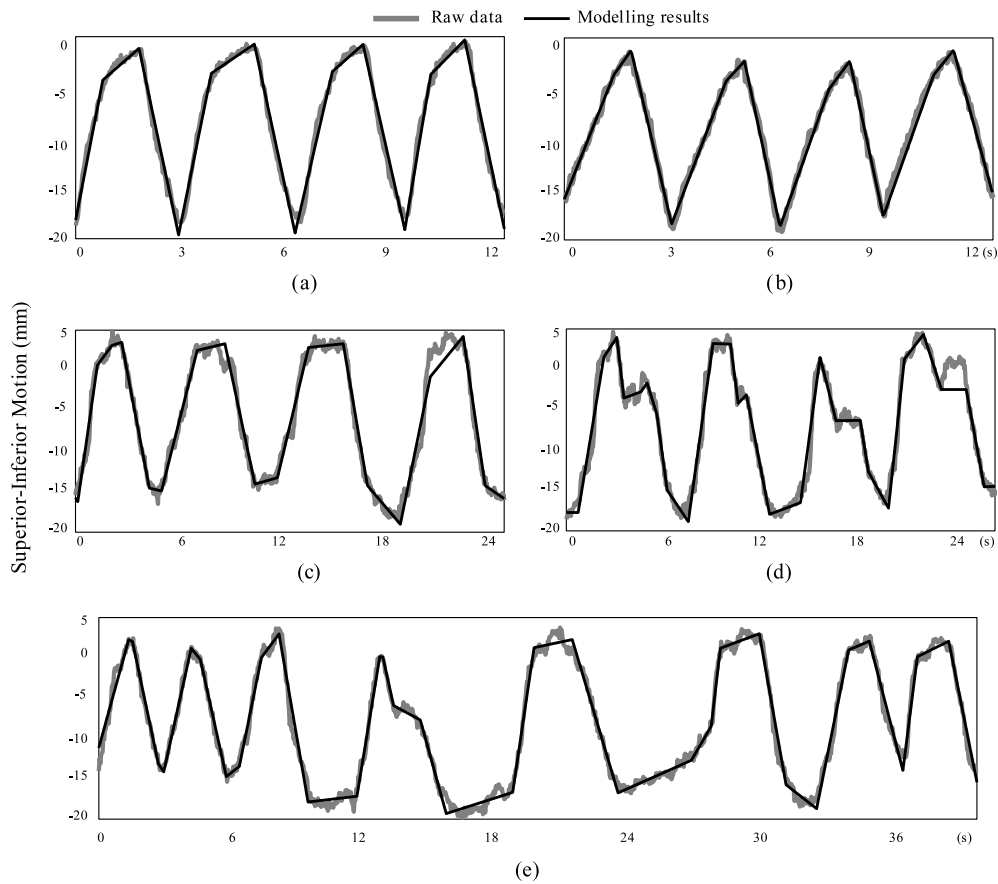


Figure 13. Modelling results for common and unusual breathing patterns: (a) three breathing states, (b) two breathing states, (c) four breathing states, (d) special breathing states and (e) combinations of all breathing states.

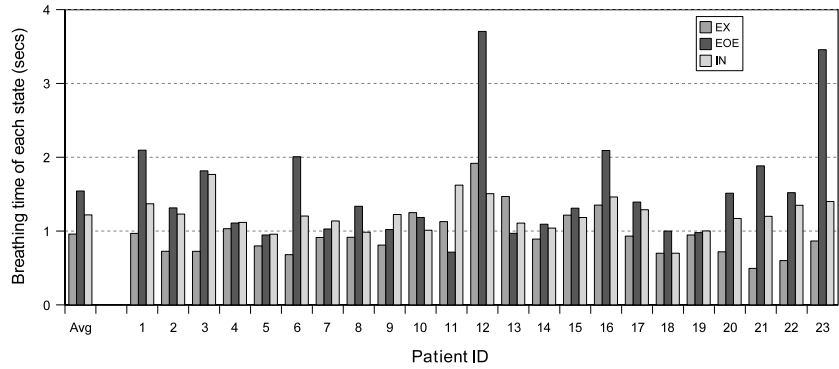


Figure 14. Average time spent in regular breathing phases.

$EX < EOE < IN$, such as patients 7 and 9. Examples of these differences are shown in figure 15.

There are a few patients with RMS errors more than 1 mm among the 23 patients shown in figure 11. One source of this error is patients whose exhale and inhale states are not quite

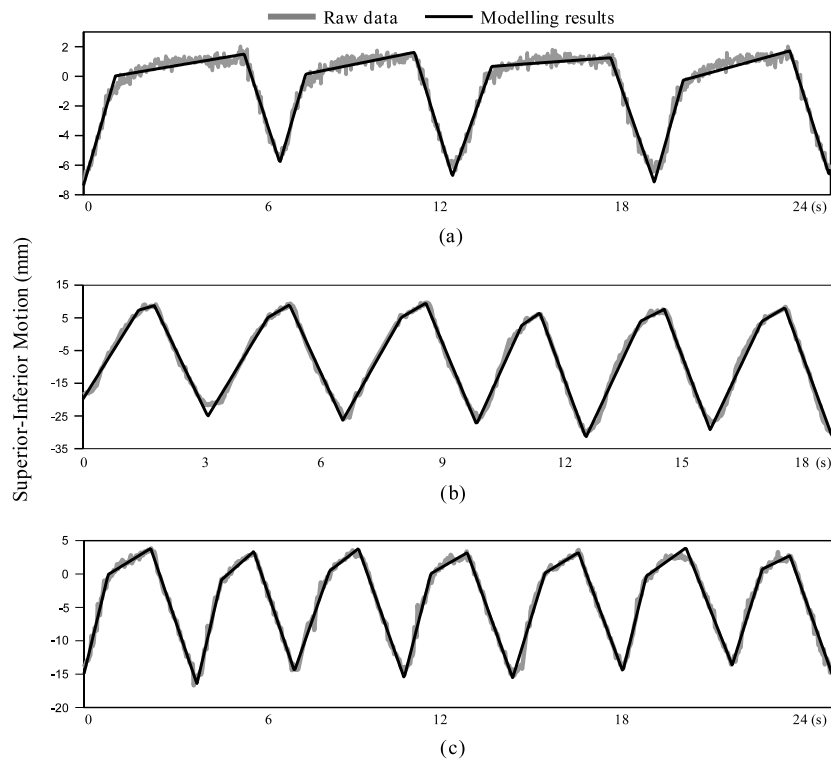


Figure 15. Different patterns of a breathing cycle: (a) longer EOE state, shorter EX and IN states, (b) shorter EOE state, longer EX and IN states and (c) lengths in the increasing order of EX, EOE and IN states.

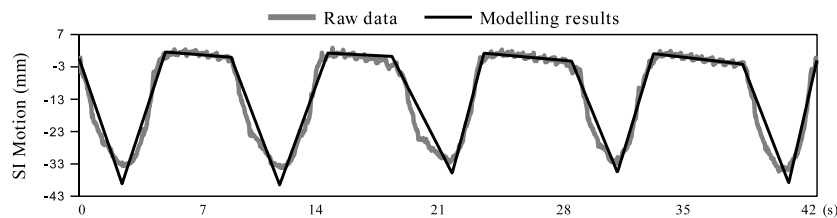


Figure 16. Nonlinear states are preferred for some breathing patterns.

linear. For example, consider the motion of patient 10, as illustrated in figure 16. Nonlinear exhale and inhale states would give a better result for this patient. Another shortcoming of our model is that it only can handle tumours with small cardiac motion. For tumours with cardiac motion more than half of the motion amplitude, our model cannot distinguish the respiratory motion from the cardiac motion. Finally, the rigid assumption of three states for one breathing period also puts limitations on the expressiveness of this model. For example, if a tumour only moves with exhale and inhale states, our method enforces the tumour to have an EOE state. It would be preferred to switch from a three-state model to a two-state model. Another example is that if a breathing period may have an additional state between the end of inhale and the beginning of exhale. Our model generates an irregular state (IRR) for the prolonged inhale state, where a four-state model will give a better understanding.

5. Conclusion

We have proposed a three-state model for respiratory tumour motion that fits the natural understanding of breathing phases, and conforms well to real patient data. We have implemented a one-dimensional version of this model in an on-line algorithm that segments the breathing signal into line segments for each state. The average root mean square error of our model is less than 1.5 mm for the patients, which demonstrates the fidelity of our model to raw data. This model and its implementation can be used for both on-line and offline data analyses. The patterns of different breathing states give useful information about patient-specific breathing. This model can be applied to internal and external motions, including tumour position, abdominal surface, diaphragm, spirometry and other surrogates.

Our future research includes several areas. One area modifies the current model to include nonlinear states, and more or less states per breathing period. We would like to address cardiac motion in the context of tumour respiratory motion. Another ongoing project is motion prediction based on the finite state model for real-time radiation therapy. A salient feature of the model is that it provides a handy base for statistics, probability analysis and database similarity matching. We are combining all these technologies in the prediction method to improve the prediction results.

Acknowledgments

This work was supported in part by NSF grant IIS-0073063, the Whitaker Foundation Grant RG-01-0175, and CenSSIS, the Center of Subsurface Sensing and Imaging Systems, under the Engineering Research Centers Program of the NSF (award number EEC-9986821).

References

- Bortfeld T and Jiang S B 2004 Effects of motion on the total dose distribution *Semin. Radiat. Oncol.* **14** 41–51
- Bortfeld T, Jokivarsi K, Goitein M, Kung J and Jiang S B 2002 Effects of intra-fraction motion on IMRT dose delivery: statistical analysis and simulation *Phys. Med. Biol.* **47** 2203–20
- Goitein M 2004 Organ and tumour motion: an overview *Semin. Radiat. Oncol.* **14** 2–9
- Jiang S B, Pope C, Aljarrah K M, Kung J, Bortfeld T and Chen G T Y 2003 An experimental investigation on intra-fractional organ motion effects in lung IMRT treatments *Phys. Med. Biol.* **48** 1773–84
- Keall P J, Kini V R, Vedam S S and Mohan R 2001 Motion adaptive x-ray therapy: a feasibility study *Phys. Med. Biol.* **46** 1–10
- Lujan A E, Larsen E W, Balter J M and Ten Haken R K 1999 A method for incorporating organ motion due to breathing into 3D dose calculations *Med. Phys.* **26** 715–20
- Mageras G S and Yorke E 2004 Deep inspiration breath hold and respiratory gating strategies for reducing organ motion in Radiation treatment *Semin. Radiat. Oncol.* **14** 65–75
- Murphy M J 2004 Tracking moving organs in real time *Semin. Radiat. Oncol.* **14** 91–100
- Neicu T, Shirato H, Seppenwoolde Y and Jiang S B 2003 Synchronized moving aperture radiation therapy (SMART): average tumour trajectory for lung patients *Phys. Med. Biol.* **48** 587–98
- Seppenwoolde Y, Shirato H, Kitamura K, Shimizu S and Adler J R 2002 Precise and real-time measurement of 3D tumour motion in lung due to breathing and heartbeat, measured during radiotherapy *Int. J. Radiat. Oncol. Biol. Phys.* **53** 822–34
- Shirato H *et al* 2000a Four-dimensional treatment planning and fluoroscopic real-time tumour tracking radiotherapy *Int. J. Radiat. Oncol. Biol. Phys.* **48** 1187–95
- Shirato H *et al* 2000b Physical aspects of a real-time tumour-tracking system for gated radiotherapy *Int. J. Radiat. Oncol. Biol. Phys.* **48** 435–42
- Suh Y, Yi B, Ahn S, Kim J, Lee S, Shin S and Choi E 2004 Aperture maneuver with compelled breath (AMC) for moving tumours: A feasibility study with a moving phantom *Med. Phys.* **31** 760–6
- van Herk M 2004 Errors and margins in radiotherapy *Semin. Radiat. Oncol.* **14** 52–64